SUPPLEMENTARY INFORMATION

Cracker method:

One sample requires 5-6 g of ice (V = $l \cdot w \cdot h$ = 2.2·1.5·2.2 cm^3). This corresponds to about 0.5 ml STP of air or 0.1 µl STP CO_2. A stainless steel needle cracker is lined up with the preconcentration system (Precon) and a Delta Plus XL mass spectrometer (MS) from ThermoFisher allowing online measurements. The ice cracker consists of a stainless steel body (57 ml) in which an array of stainless steel needles is mounted to crack the ice under vacuum at a temperature of -20°C. The released gas expands through a water trap (-70°C) into a small volume, where the gas pressure to evaluate the CO_2 concentration is measured. The extracted air is then flushed by a high helium flux of about 600 ml/min through the cracker to the Precon. This unit permits the quantitative separation of CO_2 and N_2O from air as well as switching from a high to a low helium stream (~1 ml/min). After having passed a GC (gas chromatography) column to separate CO_2 from N_2O and possible organic components, e.g. derived from drilling fluid, the CO_2 sample is injected into the MS via an open-split. During one day of measurements several runs with bubble free ice (EK) combined with a gas of known isotopic composition (EG II, $\delta^{13}C$ = -4.74‰ VPDB) are performed. These standard gas measurements allow checking the system and referencing the samples[1].

Sublimation method:

The retrieval of $\delta^{13}C$ values on CO_2 from gas enclosures in ice cores using sublimation (together with $\delta^{18}O$ and mixing ratios of CO_2 and N_2O) is split into two separate analytical systems: First, the gas extraction using sublimation in a vacuum line and secondly, a sample clean-up in a helium flow line coupled to continuous flow isotope ratio mass spectrometry (CF-IRMS).

The principle behind the gas extraction is sublimation allowing for a quantitative release of air trapped in either bubble or clathrate ice samples. Within a glass vessel, a cylindrical ice sample of 30 g is held at -25°C via a cold air stream. By illuminating the sample with infrared light a water vapour flux is established from the sample to a nearby cold trap thereby quantitatively releasing the enclosed gases. This gas stream is dried in a cold trap at -120°C and afterwards CO_2 and N_2O are separated from the major air components (N_2, O_2, Ar) at -196°C. The amount of the major air components is measured with a pressure gauge connected to a temperature controlled expansion volume. Together with the signal from the mass spectrometer the mixing ratios of CO_2 and N_2O can be calculated by referencing it to the standard gas concentrations. CO_2 and N_2O are transferred into a glass tube, which is then flame-sealed to be stored until the clean-up and measurement step. The extraction line is equipped with a gas inlet to continuously inject calibrated air samples into the sublimation vessel, thus, mimicking the continuous gas release during the sublimation of an ice sample. These air samples are used as a reference for both the isotopic measurement and the mixing ratio of CO_2 and to monitor the entire analysis.

The sample clean-up line consists of a tube cracker device to open the sealed glass tubes within a helium flux of 0.9 ml min^{-1}, a cryofocus capillary to generate a sharp sample peak and a chromatographic column to separate isobaric components (N_2O and organic components from drilling fluid) from CO_2. Finally, pure CO_2 is then admitted to a Finnigan 253 IRMS (isotope ratio mass spectrometer) via an open split interface. This off-line set-up minimizes additional uncertainty introduced by the clean

up and IRMS measurement procedure as all samples can be measured at the identical instrument conditions thus, day to day instrument variations are omitted. Like the gas extraction line, the sample clean-up line is equipped with a reference device to introduce working standards of CO_2/N_2O prior to each ice or air sample. The peak size of the working standard can be adjusted to cover the range of sample sizes thereby accounting for a potential dependency of the $\delta^{13}C$ signal on CO_2 amount[2].

Discussion of the outlier at 2.5 kyr BP

The samples with a gas age of 2,519 yr BP were not taken into account for the interpretation and for calculating splines. Air from this depth was extracted independently with the cracker as well with the sublimation method. Both methods indicate a much too negative $\delta^{13}C$ value. A closer look on the raw data of this depth interval revealed that replicate ice samples only a few cm apart (or a few years in age) show $\delta^{13}C$ variations of 0.4‰. Given the broad age distribution of the enclosed air (around 170 years) we can clearly rule out an atmospheric perturbation as cause. As the CO_2 concentration measured on the same samples deviate only by a few ppmv from neighbouring depth intervals a post drilling contamination with recent atmospheric air (with more negative $\delta^{13}C$ values and elevated CO_2 concentration) can be ruled out as well. However, just 0.3 m above this interval drilling problems occurred (E. Wolff, personal communications) likely generating extreme mechanic stress on the ice below which can be responsible for these outliers, yet the underlying process is not understood.

Gravitation correction:

As mentioned in the text, the isotopes of the enclosed air are fractionated due to gravitational settling. As a result, the heavy isotopes are concentrated at the bottom of the firn column. Accordingly, the enclosed air in the ice is enriched in heavy molecules. This fractionation depends on the mass difference of the gas species, the mean site temperature and on the diffusive column height of the firn. Since the isotopic composition of atmospheric N_2 remained constant over long time intervals, measuring $\delta^{15}N$ in air from ice cores can be used to correct $\delta^{13}C$ for the gravitation effect. Thereby, changes in $\delta^{15}N$ can directly be applied to correct $\delta^{13}C$ values since the mass differences of the involved isotopes are the same. Existing $\delta^{15}N$ data for Dome C are shown in Figure S1 (b). The single $\delta^{15}N$ value at 0 yrs BP is taken from firn measurements performed within the framework of the EU project FIRETRACC[3]. $\delta^{15}N$ values from 1 to 9 kyr BP are unpublished values measured at LSCE in 2008 (D. Rodriguez, E. Capron and A. Landais, personal communication), and $\delta^{15}N$ values after 9 kyr BP were measured at LSCE[4] in 2003. Also shown in Figure S1 are two splines of our data set, one through the uncorrected data and the other through the gravitation corrected data. The influence of the gravitation correction is summarised in Table ST1:

The main difference is the time when the $\delta^{13}C$ maximum is reached (T_{max}). Since the gravitation correction is almost constant during the Holocene, the main conclusions are not affected by this correction. Therefore, the increase in $\delta^{13}C$ by about 0.25‰ in the early Holocene and the slight decrease in the late Holocene are robust.

Comparison of extraction methods (cracker and sublimation):
Since the measurements were performed with two different extraction methods and two distinct mass spectrometers and separate standard gases, the two data sets have to be checked for a possible offset. Therefore, splines were calculated for both records (Figure S2). Additionally, Table ST2 summarises the main features of the two records including a comparison between the slopes from 11-8 kyr BP and 6-0 kyr BP. The main differences between the two records are the point of time, T_{max}, where the maximum $\delta^{13}C$ value is reached as well as the strength of the decrease after this point. Both records suggest an increase of $\delta^{13}C$ between 11-8 kyr BP. Within the error of the slopes, this increase is robust. The decrease after 6 kyr BP is slightly higher for the sublimation measurements but it is also consistent within the measurements errors.

Comparison with a former $\delta^{13}C$ record derived with the cracker method
Another unpublished $\delta^{13}C$ record over the Holocene period was already established in 2004 with a cracker system similar to the one used in this study but with a significantly higher scatter[5]. A compilation of all three records is shown in Figure S3. Within the range of error, the data derived earlier are in good agreement with the data presented in the main text except for the period from about 8 to 7 kyr. Here, the older measurements are systematically too low by about 0.4‰. So far we have not been able to find any explanation for this deviation. Since this early study, however, substantial progress has been made by constructing an improved and dedicated cracker system, and by including a gas chromatographic column which helped to significantly reduce the measuring uncertainty. Therefore, we refrain from including this data set into the discussion in the main text.

Splines for different cut-off periods:
In order to quantify the effect of different cut-off periods, splines[6] were calculated for cut-off periods between 0.5 kyr and 6 kyr (Figure S4). For periods between 0.5-1 kyr, the splines are not smooth but show millennial oscillations. Considering our uncertainty of ±0.07‰, and the time resolution of our data, these oscillations are not significant and cannot be interpreted. However, it is noteworthy that the Law Dome ice core data[7] show a wiggle that would be in line with millennial oscillations suggested by our new Holocene record. Data with further improved precision and time resolution are needed to verify or falsify such millennial-scale oscillations. For a cut-off period of more than 3 kyr, the oscillations disappear and the long-term trend as mentioned in the text becomes visible.

Mass-spectrometric CO_2 measurements:
With both of our measuring set-ups it is possible to estimate the CO_2 concentration parallel to $\delta^{13}C$ values. The CO_2 concentration can be calculated by comparing the ratio of the gas extraction pressure and the peak area of mass to charge ratio 44 in the mass spectrometer with the corresponding ratio of a standard gas. The mean

reproducibility for the cracker and sublimation methods is 2.6 ppmv and 2.9 ppmv, respectively. This is about twice as much as for the dedicated CO_2 concentration method[8]. Concerning the cracker measurements the main uncertainty lies in the behaviour of the water vapour and desorption/adsorption effects during the cracking process and the subsequent pressure measurement. Water vapour may account for a small pressure increase and possibly affects the pressure readings. In case of the concentration results from the sublimation method the pressure reading is sensitive to temperature fluctuations which may explain the larger scatter and slightly higher values. The results are presented in Figure S5 in comparison with the measurements performed on the EDC96 ice by a laser absorption spectroscopy method[9].

Model description and additional results

Model description

Model calculations were performed with an impulse response representation of the High-Latitude Exchange/Interior Diffusion-Advection (HILDA) ocean model coupled to a 4-box representation of vegetation and soils and a well-mixed atmosphere[10]. Carbonate compensation is included by assuming that a fraction, *a*, of 70% of the terrestrial release (uptake) is absorbed by sediments on an exponential timescale, τ, of 5 kyr[11, 12]. A $^{13}C/^{12}C$ fractionation of 18.7‰ is applied for the atmosphere-to-land biosphere flux and fractionation for fluxes between atmosphere and surface ocean are from Mook[13] as described elsewhere[14].

Mass-balance inverse model calculations

Carbon fluxes in the land biosphere-only scenario (S_1) are quantified by a (single) deconvolution of the atmospheric CO_2 record[15]. Atmospheric CO_2 is prescribed and carbon uptake by the ocean-sediment system is simulated. The total carbon inventory in the atmosphere-land biosphere-ocean-sediment system remains constant. Then, the net land biosphere-to-atmosphere flux is equal to the prescribed change in the atmospheric carbon inventory and the calculated ocean uptake flux. The land biosphere-global SST (SST: sea surface temperature) scenario (S_2), the land biosphere-marine biosphere scenario (S_3), and the land biosphere-marine carbonate compensation scenario (S_4) are quantified by (double) deconvolutions of the atmospheric CO_2 and $\delta^{13}C$ records as detailed by Joos and Bruno[14] and Indermühle et al.[11]. In the land biosphere-global SST scenario, the partial pressure of CO_2 in the surface ocean is forced to be consistent with the inferred net sea-to-air flux (from the mass balance of CO_2 and $^{13}CO_2$) and the prescribed atmospheric CO_2 by adjusting global SST in the model. The isotopic fractionation for the air-sea and sea-air fluxes is evaluated for the adjusted global SST. In the land biosphere-marine biosphere scenario, the surface ocean CO_2 partial pressure is similarly adjusted by adding (removing) dissolved inorganic carbon that is depleted in $\delta^{13}C$ by 20‰ relative to the surface ocean ^{13}C to ^{12}C ratio. In the land biosphere-carbonate compensation scenario, the surface partial pressure is adjusted without modification of the ^{13}C to ^{12}C ratio. The small fractionation of ~1‰ that occurs during calcium carbonate formation is neglected.

The land biosphere-global SST scenario S_2 yields a net carbon flux of about 190 GtC to the terrestrial biosphere from 11-6 kyr BP and a decrease of the terrestrial biosphere of 120 GtC from 6-0 kyr BP (Figure S6). Derived global SST indicates an

increase by about 1.5°C over the Holocene, which is unrealistic. The double deconvolution for the land biosphere-marine biosphere scenario S_3 leads to unrealistically high terrestrial carbon fluxes and requires an increase of the terrestrial biosphere of about 700 GtC from 11-3.5 kyr BP followed by a decrease of 100 GtC from 3.5-0 kyr BP. Such large fluxes and the large increase in the terrestrial biosphere during the Holocene are most unlikely and in contrast to vegetation model estimates[12] and pollen-based reconstructions of vegetation cover[16]. However, we can not entirely exclude that marine biological processes have contributed to the co-evolution of atmospheric CO_2 and $\delta^{13}C$.

Sensitivity of simulated CO_2 to the timescales of carbonate compensation and the temporal evolution terrestrial carbon uptake during the transition

Model simulations were performed to project atmospheric CO_2 from prescribed land biosphere-atmosphere fluxes to evaluate whether the results of the mass balance inverse calculation for the land biosphere-carbonate scenario are plausible. The sensitivity of simulated CO_2 to changes in the following parameters is addressed: carbonate compensation timescale τ; the fraction *a* of the perturbation to be mitigated by carbonate compensation, and the uptake history of the terrestrial biosphere. Four different schematic uptake histories prior to the Holocene are selected and shown in Figure S7: (i) no land biosphere uptake during the Transition to detect the effect of the carbonate compensation caused by the land biosphere uptake during the early Holocene; (ii), the standard uptake that assumes a linear increase in the land biosphere inventory of 700 GtC during the Transition in 7 kyr (constant flux of 0.1 GtC yr^{-1} from 18 to 11 ka BP); (iii), a rapid land biosphere uptake of 700 GtC in 2 kyr; and (iv), a slow land biosphere uptake of 700 GtC in 10 kyr. The CO_2 decrease in the early Holocene is stronger and the increase during the late Holocene is smaller for the 10 kyr uptake history compared to the standard. A rapid but intense uptake history during the Transition (iii) results in a stronger increase of CO_2 during the late Holocene. The measured atmospheric CO_2 data are simulated better when τ is set to 7 kyr and the fractionation *a* is increased to 0.8. Good agreement with the data in these still very simplified scenarios results for τ = 8 kyr, *a* = 0.8 and assuming a rapid and large land biosphere uptake during the period 13 to 11 kyr BP. This reflects a scenario with a small role of coral reef buildup for Holocene CO_2.

References:

Elsig, J. *New insights into the global carbon cycle from measurements of CO_2 stable isotopes: methodological improvements and interpretation of a new EPICA Dome C ice core $\delta^{13}C$ record*. PhD Thesis, Climate and Environmental Physics, Physics Institute, University of Bern, 1-174 (2009).

Schmitt, J. *A sublimation technique for high-precision $\delta^{13}C$ on CO_2 and CO_2 mixing ratio from air trappes in deep ice cores*. PhD Thesis, Fachbereich Geowissenschaften, Universität Bremen, 1-167 (2006).

FIRETRACC. in Part C: Scientific Report (European Commission DGX, Environment and Climate, 2000).

Dreyfus, G. *Dating an 800,000 year antarctic ice core record using the isotopic composition of trapped air*. PhD thesis, Departement of Geoscience, Princeton University (2008).

Eyer, M. *Highly resolved $\delta^{13}C$ measurements on CO_2 in air from Antarctic ice cores*. PhD Thesis, Climate and Environmental Physics, Physics Institute, University of Bern, 1-113 (2004).

Enting, I. G. *On the Use of Smoothing Splines to Filter CO_2 Data*. Journal of Geophysical Research-Atmospheres **92**, 10977-10984 (1987).

Francey, R. J. et al. *A 1000-year high precision record of $\delta^{13}C$ in atmospheric CO_2*. Tellus Series B-Chemical and Physical Meteorology **51**, 170-193 (1999).

Lüthi, D. et al. *High-resolution carbon dioxide concentration record 650,000-800,000 years before present*. Nature **453**, 379-382 (2008).

Monnin, E. et al. *Atmospheric CO_2 concentrations over the last glacial termination*. Science **291**, 112-114 (2001).

Joos, F. et al. *An efficient and accurate representation of complex oceanic and biospheric models of anthropogenic carbon uptake*. Tellus Series B-Chemical and Physical Meteorology **48**, 397-417 (1996).

Indermühle, A. et al. *Holocene carbon-cycle dynamics based on CO_2 trapped in ice at Taylor Dome, Antarctica*. Nature **398**, 121-126 (1999).

Joos, F., Gerber, S., Prentice, I. C., Otto-Bliesner, B. L. & Valdes, P. J. *Transient simulations of Holocene atmospheric carbon dioxide and terrestrial carbon since the Last Glacial Maximum*. Global Biogeochemical Cycles **18**, 1-18 (2004).

Mook, W. G. *^{13}C in Atmospheric CO_2*. Netherlands Journal of Sea Research **20**, 211-223 (1986).

Joos, F. & Bruno, M. *Long-term variability of the terrestrial and oceanic carbon sinks and the budgets of the carbon isotopes ^{13}C and ^{14}C*. Global Biogeochemical Cycles **12**, 277-295 (1998).

Bruno, M. & Joos, F. *Terrestrial carbon storage during the past 200 years: A Monte Carlo analysis of CO_2 data from ice core and atmospheric measurements*. Global Biogeochemical Cycles **11**, 111-124 (1997).

Prentice, I. C., Jolly, D. & participants, B. *Mid-Holocene and glacial-maximum vegetation geography of the northern continents and Africa*. J. Biogeogr **27**, 507–519 (2000).

Tables:

	$\delta^{13}C_{min}$ (‰)	$\delta^{13}C_{max}$ (‰)	T_{max} (‰)	$\delta^{13}C_{end}$ (‰)	(11-T_{max}) kyr BP increase (‰)	(T_{max}-T_{end}) kyr BP decrease (‰)
(1) uncorrected	-6.07	-5.83	6116	-5.89	0.24	-0.06
(2) corrected	-6.58	-6.33	5535	-6.38	0.25	-0.05

ST1: Summary of the main features of the spline through the uncorrected data set (1) and through the gravitation corrected data set (2). T_{max} is the year BP where the spline through the data reaches its maximum $\delta^{13}C$ value whereas $\delta^{13}C_{end}$ refers to the value of the spline for the most recent sample.

	$\delta^{13}C_{min}$ (‰)	$\delta^{13}C_{max}$ (‰)	T_{max} (‰)	$\delta^{13}C_{end}$ (‰)	11-8 kyr BP increase (‰/kyr)	6-0 kyr BP decrease (‰/kyr)
(1) cracker	-6.60	-6.32	5750	-6.35	-0.06±0.02	0.01±0.01
(2) sublimation	-6.64	-6.32	4800	-6.43	-0.07±0.03	0.018±0.009

ST2: Summary of the main features of the spline through the cracker data record (1) and through the sublimation data record (2) as well as the comparison between the linear slopes through the individual records and their uncertainties for the intervals 11-8 kyr BP and 6-0 kyr BP. T_{max} is the year BP where the spline reaches its $\delta^{13}C$ maximum whereas $\delta^{13}C_{end}$ refers to the value of the spline for the most recent sample.

Figures:

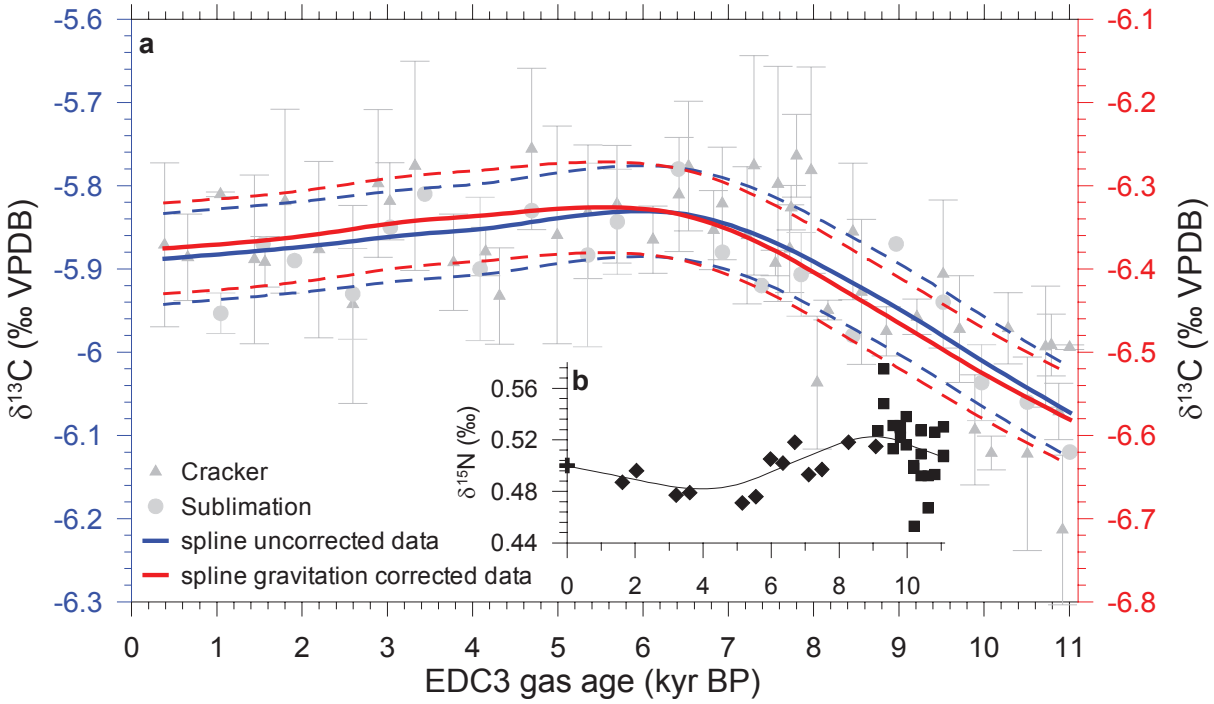

Figure S1: The effect of the gravitation correction on the $\delta^{13}C$ record. (a) The blue line is the spline through the uncorrected data set (left y-axis) with its 1σ uncertainty band (dashed line), whereas the red line corresponds to the spline through the gravitation corrected data set (right y-axis) with its corresponding 1σ band. (b) The inset corresponds to $\delta^{15}N$ data. The single $\delta^{15}N$ value at 0 yrs BP is taken from firn measurements (black cross)[3]. $\delta^{15}N$ values from 1 to 9 kyr BP are unpublished values measured at LSCE by D. Rodriguez, E. Capron and A. Landais in 2008 (black diamonds), and $\delta^{15}N$ values after 9 kyr BP were measured at LSCE by G. Dreyfus in 2003 (black squares). A spline through the $\delta^{15}N$ data was used to correct the $\delta^{13}C$ data. This spline indicates a mean correction of (0.50 ± 0.01)‰. Within the error band, the two splines through the $\delta^{13}C$ data agree. Therefore, the main conclusions of this paper are not affected by the gravitation correction.

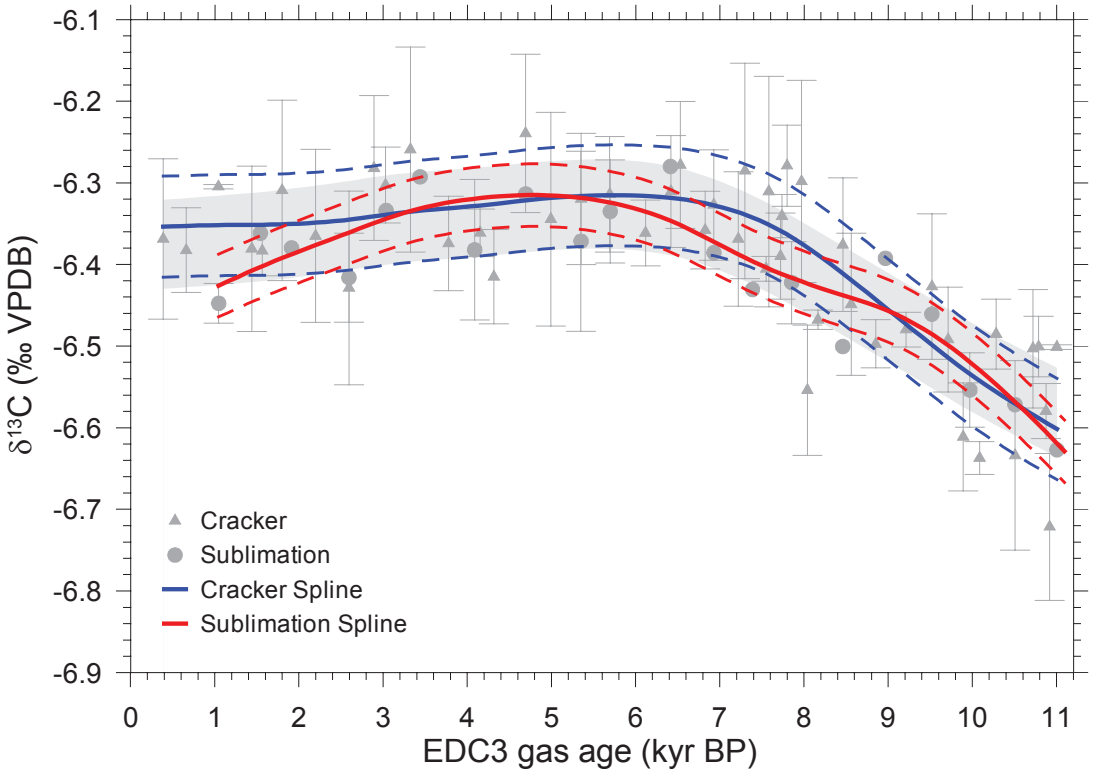

Figure S2: Spline through the cracker data set (blue line) with 1σ error band and the spline through the sublimation data set (red line). The grey shaded area is the 1σ band of the spline through both data sets. The two splines agree within their uncertainties. Therefore, an offset of the methods can be excluded.

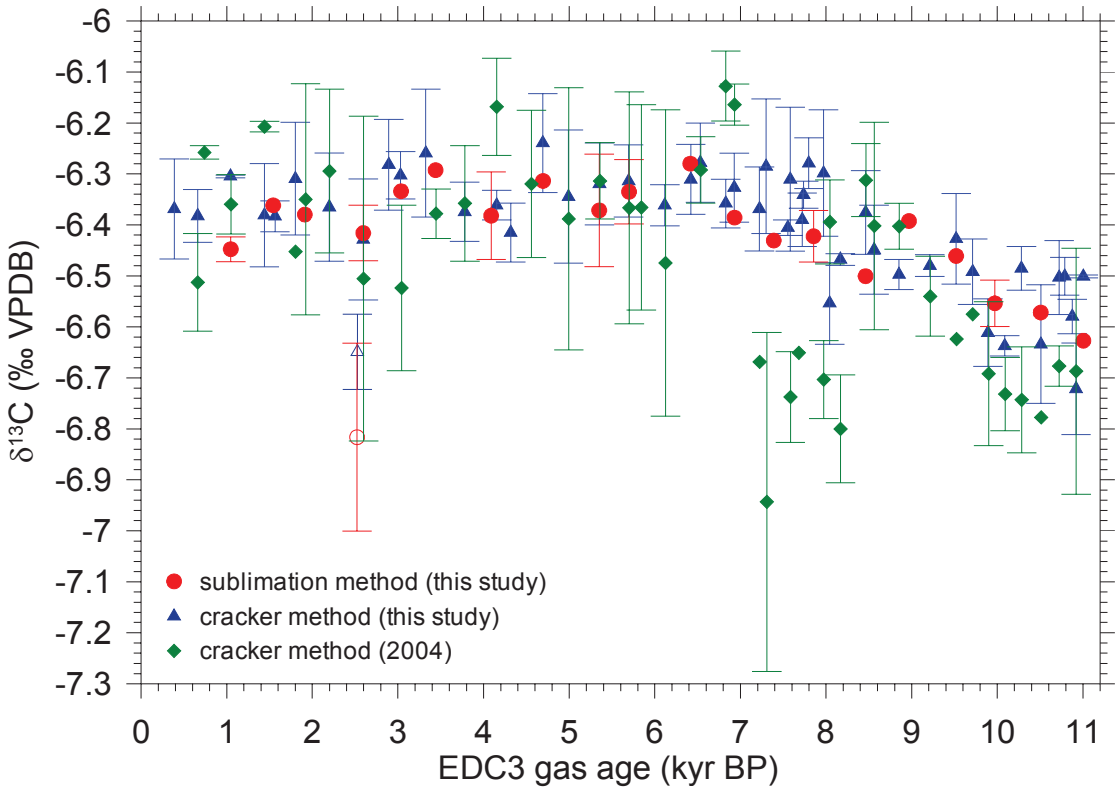

Figure S3: Comparison of the $\delta^{13}C$ data from this study with unpublished data (green diamonds, mean of mostly two samples, error bars are 1σ of the mean) established in 2004 in Bern[5] with a preliminary cracker method compared to the one used in this study.

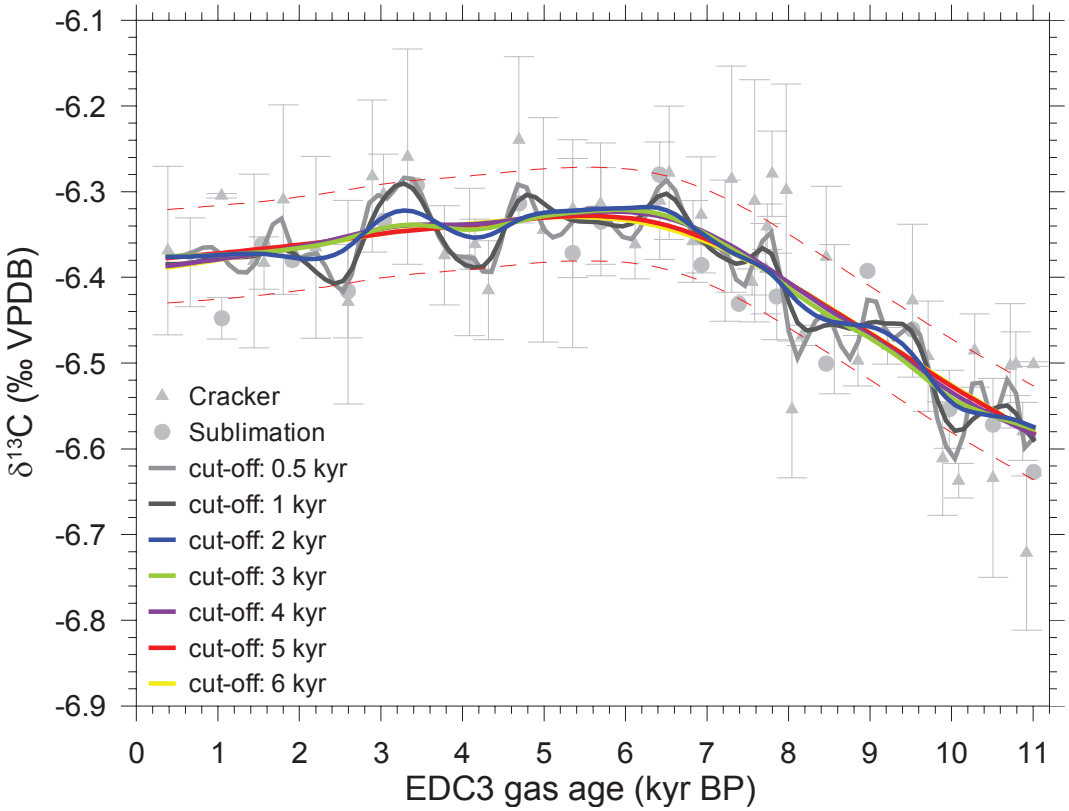

Figure S4: Splines of Monte-Carlo simulations with different cut-off periods. For cut-off periods longer than about 3 kyr, the oscillating behaviour of the splines disappears and the long-term trend becomes robust. The dashed red lines indicate the 1σ band of the spline with a cut off period of 5 kyr.

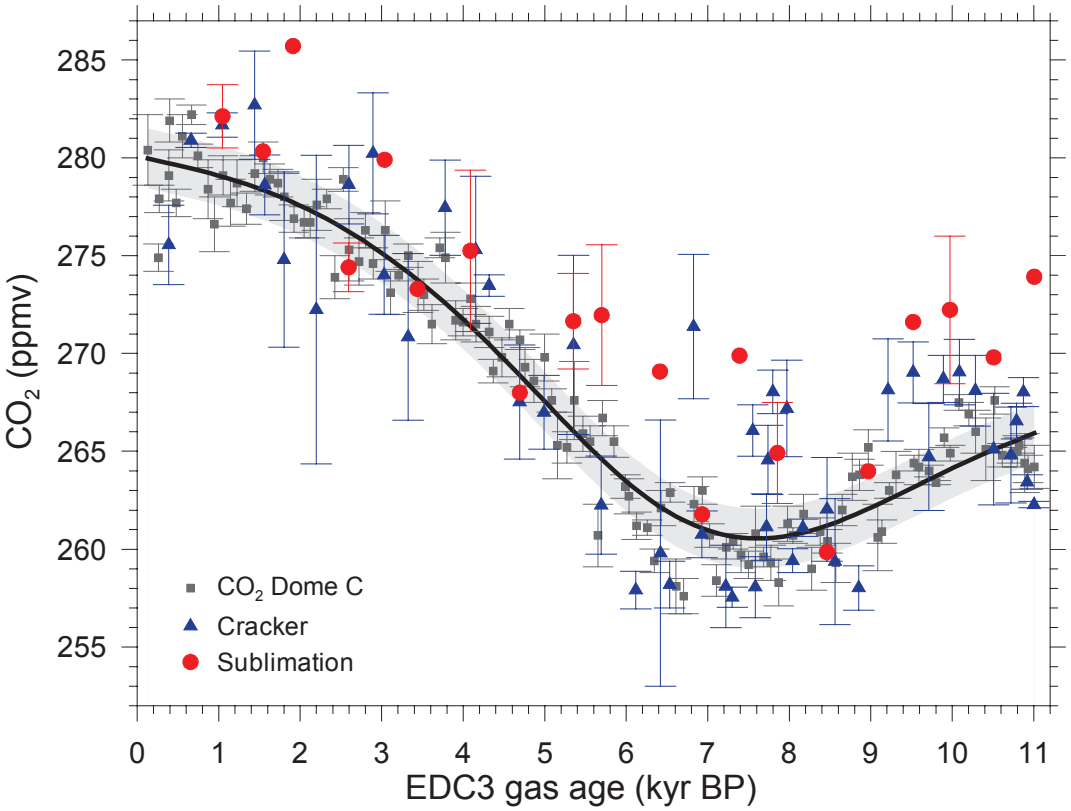

Figure S5: CO_2 record of air trapped in Dome C ice. Blue triangles are the measurements performed with the cracker set-up. Red circles are CO_2 concentration measurements obtained using the sublimation set-up. The error bars represent the t-weighted 1σ standard deviation of the mean. Grey squares are the CO_2 measurements from Monnin et al.[9]. The black line is the spline through the record of Monnin et al. with a cut-off period of 5 kyr and the grey shaded area is the corresponding 1σ band.

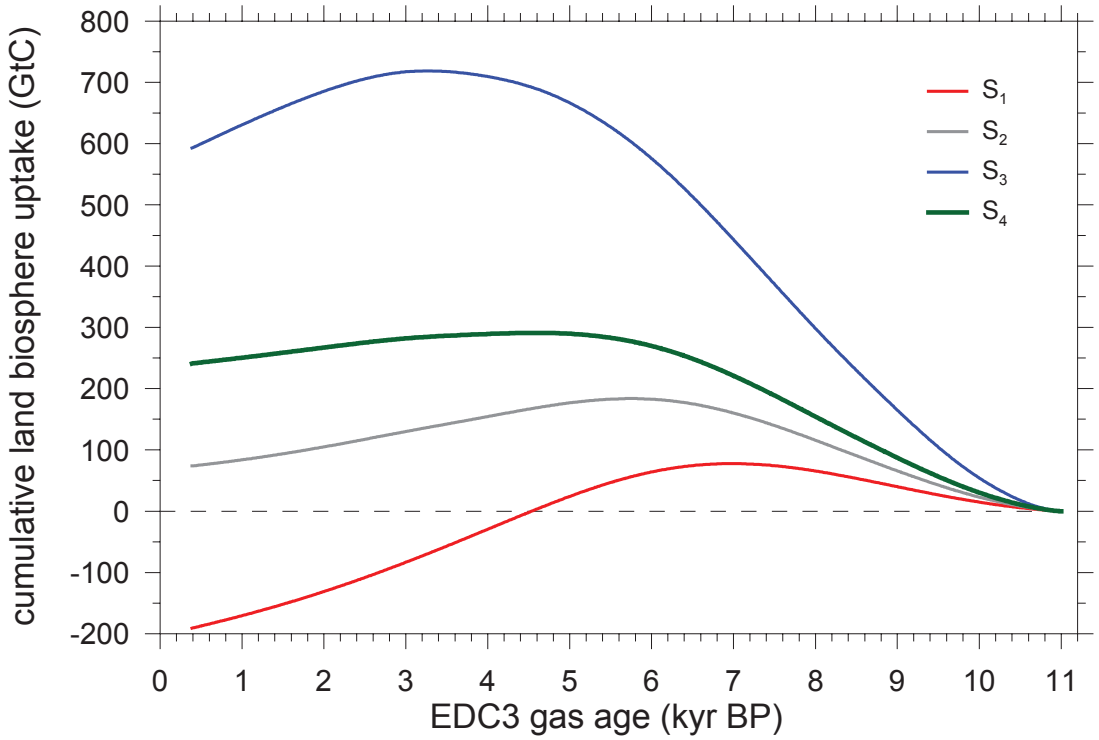

Figure S6: Cumulative land biosphere uptake from inverse modelling results for the discussed scenarios: (S_1: land-biosphere-only scenario, S_2: land biosphere-global SST scenario, S_3: land biosphere-marine biota scenario, S_4: land biosphere-marine carbonate compensation scenario).

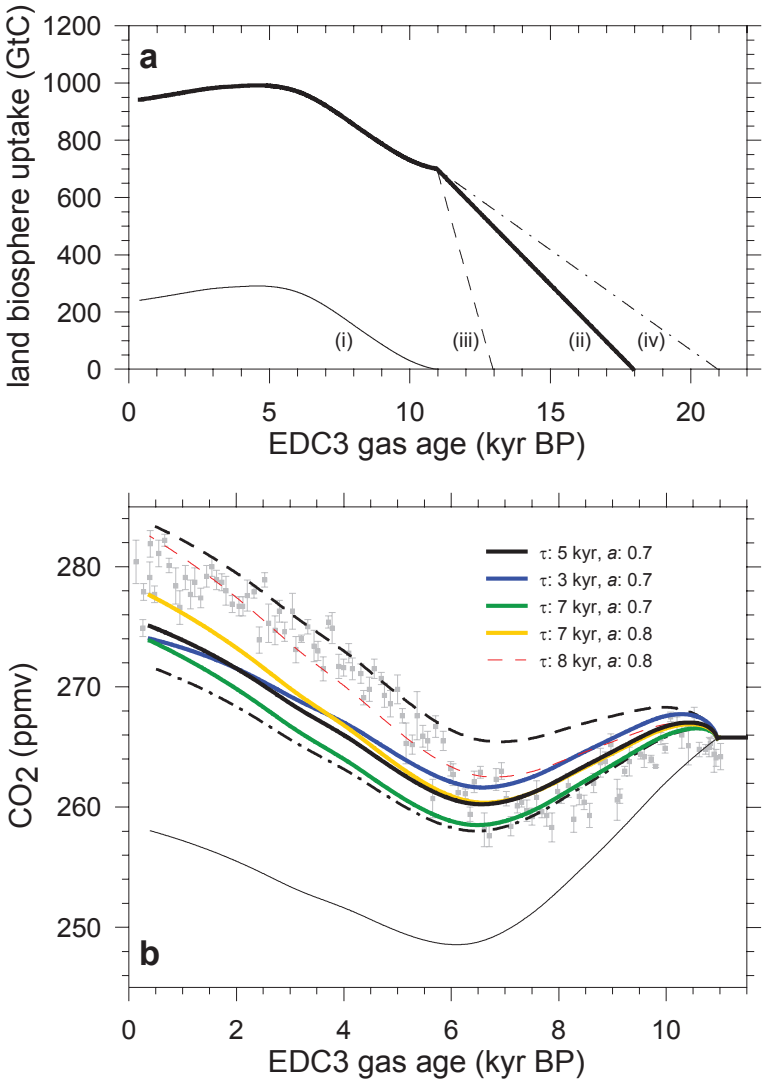

Figure S7: Sensitivity tests for the CO_2 evolution predicted by the land biosphere-marine carbonate compensation scenario S_4 during the Holocene. a) During the Transition, the cumulative land biosphere uptake of 700 GtC is prescribed by a linear increase in 7 kyr (thick black line, (ii)), in 2 kyr (dashed black line, (iii)) or in 10 kyr (dash-dotted black line, (iv)). After 11 kyr BP, the land biosphere uptake is dictated by the output of S_4. The black thin line shows the case where no terrestrial uptake took place over the Transition (i). b) The line character is given by the different uptake histories presented left whereas the colour describes the influence of changing τ and a.